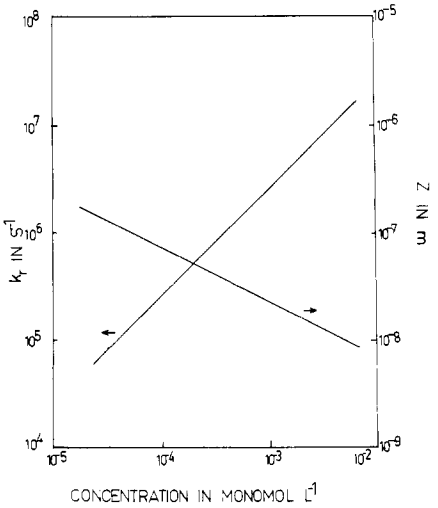


**Figure 3.** Values of $K$ as calculated in ref 5 (left scale) and the corresponding values of $Z$ (right scale) as function of monomolar concentration.

expected if the contour length of the polyelectrolyte increases above 100 nm, provided the charged macromolecule remains rodlike.

It thus seems that counterion exchange may be an important phenomenon for understanding the dielectric properties of polyelectrolytes in solution. The importance of this conclusion may strongly depend, however, on the validity of the model used to reach it. As indicated above, the two-phase model is a highly simplified approach which in the case of the electric polarizability leads to the neglect of the contribution of a certain fraction of the counterions to the dielectric properties of the solution and implies the neglect of the influence of concentration gradients on the dipole moment. The least that one can conclude from the present calculation, however, is that the two-phase model, without considering counterion exchange between the two phases, may be limited, for rodlike polyelectrolytes, to molecules not exceeding a certain length, depending on $Z$. Above this critical contour length the simple description without counterion exchange breaks down, thus eventually affecting the $L$ dependence of both the polarizability and relaxation time of the induced electric moment. In a recent paper[6] Fixman, starting from a different and more general model, has derived an expression for the dipole moment of a cylindrical polyion which has a functional dependence on $L$ comparable to our eq 9, although the quantity $Z$ in his theory is defined quite differently.

At present there are no experimental data available on systems that fulfill the necessary conditions to test this more general conclusion or those of the preceding section. To satisfy the assumptions underlying the model, the charged macromolecule should at least be rodlike in a wide range of molar masses and at concentrations where the dielectric effects still can be measured. For most polyelectrolytes this cannot be realized simultaneously. Moreover, in order to reduce the influence of concentration gradients in the free phase and of intermolecular interactions, addition of low molecular salt might be necessary, but this in turn may not be without effect on the average conformation of the macromolecule and on the sensitivity of the dielectric measurements. Therefore although in principle an experimental verification of the theoretical prediction seems to be possible, in practice many experimental problems may still have to be overcome. Hopefully in the near future new experiments will be designed which will give a decisive answer to the question whether the approach used in the present work is useful or not.

## References and Notes

(1) Oosawa, F. "Polyelectrolytes"; Marcel Dekker: New York, 1971; p 51.
(2) Minakata, A. *Ann. N.Y. Acad. Sci.* **1977**, *303*, 107.
(3) van der Touw, F.; Mandel, M. *Biophys. Chem.* **1974**, *2*, 218.
(4) Mandel, M. *Mol. Phys.* **1961**, *4*, 489.
(5) van Dijk, W.; van der Touw, F.; Mandel, M., to be submitted for publication.
(6) Fixman, M. *Macromolecules* **1980**, *13*, 711.

# Critical Evaluation of Electron Microscopy of Ionomers

**Dale L. Handlin, William J. MacKnight,* and Edwin L. Thomas**

*Polymer Science and Engineering Department, University of Massachusetts, Amherst, Massachusetts 01003.* *Received December 2, 1980*

ABSTRACT: Electron microscopy has been used to examine the morphology of four ionomers. The transfer theory of imaging, which has been overlooked in previous ionomer studies, has been used to interpret the images of both solvent-cast and microtomed thin films. Solvent casting was found to produce a number of interesting artifacts but no useful information about ionic domains. Microtomed sections of a copolymer of ethylene and methacrylic acid, sulfonated polypentenamer, and sulfonated polystyrene contained no preparative artifacts but showed no distinct domain structure even in the ionomers neutralized with cesium, probably because of film thickness problems. Microtomed sections of sulfonated EPDM, however, contain 300-nm phase-separated regions. Osmium tetraoxide staining of these EPDM sections showed domains averaging less than 3 nm in size primarily inside these regions. Unfortunately, the section thickness prohibits an accurate determination of the size distribution or the detailed shape of these domains and hence the selection of the most appropriate model of domain structure.

## Introduction

Ionomers have gained commercial importance in recent years due to the beneficial change in mechanical and ion transport properties obtained by adding a small number of ionic groups to a nonionic polymer. The copolymerization of ethylene with less than 10 mol % of methacrylic acid (E–MAA) and then neutralization with a metal cation inhibit spherulite formation, producing a material which behaves as if cross-linked at room temperature but is melt processable.[1] Incorporation of neutralized sulfonate groups into rubbers such as polypentenamer or EPDM also yields polymers with thermally

0024-9297/81/2214-0795$01.25/0 

labile "ionic cross-links". It has been suggested that the ionic groups microphase separate to form clusters or "domains", the nature of which is not well understood.

Small-angle X-ray scattering of ionomers generally shows a scattering peak near $h = 0.28$–$0.68$ Å$^{-1}$ ($h = (4\pi/\lambda) \sin\theta$, where $\theta$ is one-half the scattering angle) and strong lower angle scattering.[2-5] Small-angle neutron scattering of $H_2O$- and $D_2O$-impregnated ionomers also shows a scattering peak in this angular region,[6,7] indicating a heterogeneous distribution of electron density possibly due to 0.3–5-nm domains.

Several models have been proposed to fit the scattering data: 1.

1. Lamellar Model. Lamellae containing ionic groups are suggested to be 0.8-nm thick and are separated by hydrocarbon lamellae 2.5-nm thick. Small packets consisting of approximately five ionic and hydrocarbon lamellae are located randomly throughout the polymer.[8]
2. Shell-Core Model. A core of ions 0.6–2.6 nm in diameter is surrounded by hydrocarbon chains with a diffuse shell of ionic groups approximately 2.5 nm from the core.[9]
3. Random Lattice Model. Ionic clusters 0.5–1 nm in diameter are proposed to form a randomly disordered lattice with an average spacing of 2.5 nm.[4]

Attempts to image ionic domains directly, using electron microscopy to determine the shape and size distribution, have yielded varied results. Davis et al. found that a dilute solution of E–MAA copolymers formed spherulitic films when cast onto water but formed nonspherulitic films containing 15-nm "granularity" when cast on solutions of dilute bases.[10] Koutsky et al., however, claimed visualization of domains of 1.3–2.6-nm diameter in solution-cast films of the acid and salt forms of butadiene–methacrylic acid copolymers, both unstained and stained with osmium tetraoxide.[11] Using a polyethylene with phosphonic acid side groups, Phillips observed 5–8-nm ionic domains and 80-nm hydrogen-bonded clusters in microtomed sections stained by solvents containing cesium hydroxide or cesium acetate.[12] Pineri found a distribution of cluster sizes ranging from 150 to less than 10 nm, with most clusters having a diameter less than 10 nm, in ferric salts of a poly(butadiene–styrene–4-vinylpyridine) terpolymer.[13]

These electron microscopy studies suggest that a wide variation of domain type and size may exist, depending on the particular ionomer. On the other hand, the SAXS patterns of ionomers are very similar.

We have undertaken a study of the following four ionomers: (1) copolymer of ethylene and methacrylic acid; (2) sulfonated polypentenamer; (3) sulfonated polystyrene; (4) sulfonated EPDM. These polymers represent the spectrum of crystallizable, rubbery, glassy, and blocky backbones, respectively. A comparison of solution-cast and ultramicrotomed sections was made for one ionomer, E–MAA, and the other three were prepared for observation by ultramicrotomy. Cesium salts of these ionomers were used to enhance bright field electron microscopy amplitude contrast and small-angle X-ray scattering. High-resolution transmission images of these polymers were interpreted by using the transfer theory of imaging, which has been neglected in previous ionomer electron microscopy studies.

## Transfer Theory of Image Formation

Two types of contrast can arise in transmission electron microscope (TEM) images: amplitude contrast and phase contrast. If fluctuations in density, atomic number, or thickness are present in the object, the resulting amplitude contrast may be interpreted intuitively at medium resolution. Under high-resolution conditions or if amplitude contrast is not dominant, as is the case in most unstained polymers, images must be interpreted by utilizing transfer theory. This theory has been developed in detail in many articles[14-17] and applied to polymers in a simplified form.[18,19] (An error is present in ref 18 and 19: $\chi(\mathbf{K})$ should be replaced with $-\chi(\mathbf{K})$ in all equations.) Here we briefly outline the salient features necessary to appreciate the problems of the visualization of ionic domains.

If the amplitude of the electron wave is not altered significantly by the object, then the object function, $\psi(\mathbf{r})$, can be described just by a phase term, $\exp[i\psi(\mathbf{r})]$.[20] Further, for a weak phase object (following the first Born approximation[17]) the object function may be approximated as

$$\exp[i\psi(\mathbf{r})] \simeq 1 + i\psi(\mathbf{r}) \tag{1}$$

For this case the image intensity, $I(\mathbf{r})$, is just the inverse Fourier transform ($F^{-1}$) of a $\delta$ function and a term involving the Fourier transform of the object function modulated by the microscope transfer function $T(\mathbf{K})$:

$$I(\mathbf{r}) = F^{-1}[\delta(\mathbf{K}) - 2T(\mathbf{K})F\{\psi(\mathbf{r})\}] \tag{2}$$

Here $\mathbf{K}$ is the reciprocal space scattering vector and

$$T(\mathbf{K}) = A(\mathbf{K}) \sin[-\chi(\mathbf{K})] \tag{3}$$

$A(\mathbf{K})$ is one inside the objective aperture and zero outside, and the phase shift $\chi(\mathbf{K})$ (neglecting coherence and chromatic abberration effects) is given by

$$\chi(\mathbf{K}) = \pi\lambda(\Delta Z)\mathbf{K}^2 + (\pi/2)C_s\lambda^3\mathbf{K}^4 \tag{4}$$

where $\Delta Z$ and $C_s$ are the defocus and spherical aberration coefficient of the objective lens. The image contrast, $(I(\mathbf{r}) - I_{av})/I_{av}$, is simply

$$(I(\mathbf{r}) - I_{av})/I_{av} = F^{-1}\{2A(\mathbf{K}) \sin \chi(\mathbf{K})F[\psi(\mathbf{r})]\} \tag{5}$$

where $\mathbf{r}$ and $\mathbf{K}$ are two-dimensional vectors.

Sin $\chi(\mathbf{K})$ is a sensitive function of defocus, as shown in Figure 1, and is nearly antisymmetric with respect to focus at medium and larger defocus. Because sin $\chi(\mathbf{K})$ alternately selects or suppresses the contribution of various object spatial frequencies to the final image, a weak phase object (an amorphous carbon or polymer film with a smoothly varying $F[\psi(\mathbf{r})]$ distribution is a good example) will exhibit a "salt and pepper" structure. The size of this phase contrast structure is dependent on the microscope optical conditions employed and can be measured by taking an optical transform of the image as shown in Figure 2. The position of the maxima and minima in this optical Fourier transform is determined by the $\sin^2 \chi(\mathbf{K})$ function. The largest phase contrast structures in the image correspond to the first maximum of $\sin^2 \chi(\mathbf{K})$. Thus, from eq 4, for a defocus value of $\Delta Z$ a phase contrast structure of approximately $(2\lambda\Delta Z)^{1/2}$ appears in the image. This explains why in an early ionomer paper a defocus of 5 $\mu$m "enhance(d) the electron phase contrast" but made the results difficult to interpret.[10] This value of defocus would not only cause large fringes around the 15-nm granular structure cited, providing more contrast, but would also produce strong 6–8-nm phase contrast structures confounding the image.

The above treatment has neglected the effects of beam coherence and chromatic aberration. These effects have been shown to damp the oscillations of the transfer function, especially at large $K$.[15] The optical transforms demonstrate the importance of these effects by the limited number of maxima recorded. Optical transforms are also useful for detecting the presence of specimen drift and objective lens astigmatism in an image by the noncircu-

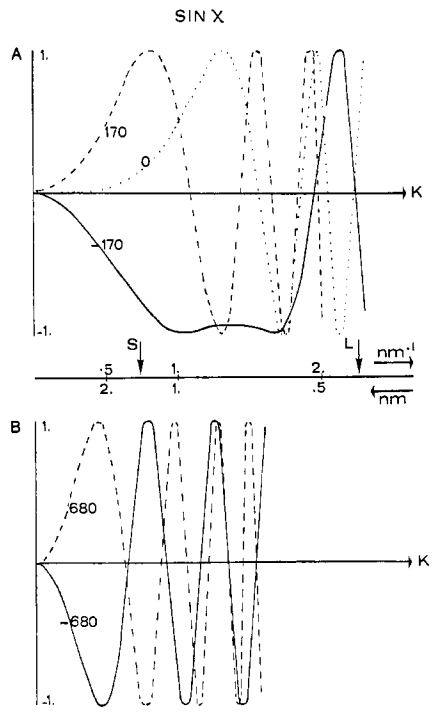


**Figure 1.** Variation of sin $\chi(\mathbf{K})$ with defocus (indicated on the curve) $C_s$ = 6.7 nm. Arrows indicate the largest **K** value accepted by the 28- (S) and 85-$\mu$m (L) objective apertures. A negative value of this function will result in a decrease in intensity ("dark" contrast) for the corresponding spacings in the image.

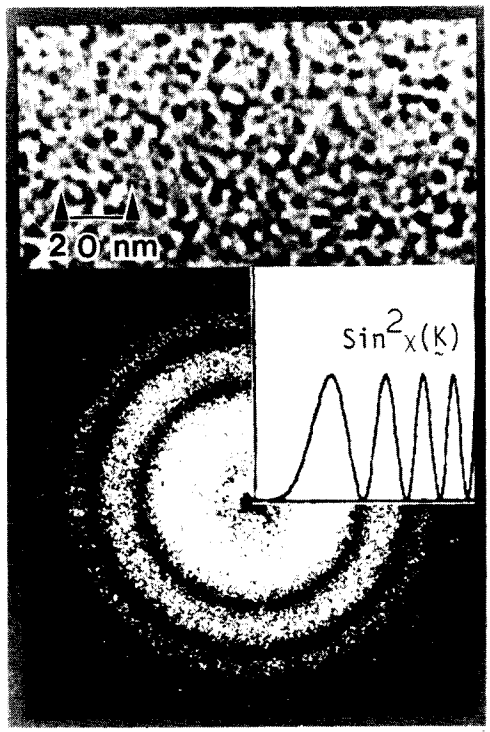


**Figure 2.** Bright field image of carbon film defocused −2600 nm. $\text{Sin}^2\ \chi(\mathbf{K})$ is shown on the optical transform of the image.

larity of the transform, as well as determining the objective lens defocus from eq 3 and 4.

Any amplitude contrast in the image will be modulated by the phase contrast, causing a confusion in the small-scale image structure for defocus conditions. Figure 3 shows a through-focus series of a thin amorphous carbon film with many osmium particles on its surface. At approximately zero defocus sin $\chi(\mathbf{K})$ is nearly zero for a wide range ($0 < K < 0.8$ nm$^{-1}$) of object frequencies (Figure 1) so that the phase contrast contributions from the amorphous carbon support film on the >1-nm scale is minimal. This permits a reasonably accurate determination of the osmium particles' size and shape from their residual amplitude contrast (Figure 3C). As the microscope is defocused, it becomes more difficult to distinguish the size and shape of the small particles due to the increased phase contrast contribution from the substrate. The contribution of phase contrast increases with the amount of objective lens defocus and is already comparable to the amplitude contrast of the osmium particles at a defocus of only 1100 nm. The antisymmetry of sin $\chi(\mathbf{K})$ (see Figure 1) with defocus leads to a reversal in contrast of the phase contrast structure of the carbon support and produces black fringes around osmium particles for overfocus conditions, which become white fringes when underfocus (Figure 3A,E). By taking a through-focus series of micrographs, however, one can distinguish amplitude contrast from phase contrast. Unfortunately, dark regions in a single image containing unknown contributions from phase contrast and amplitude contrast have been previously erroneously interpreted as arising from ionic domains in ionomers,[11] as well as segmented hard and soft domains in urethanes[21-23] and nodular structures in amorphous homopolymers.[24-30]

The large difference in scattering power for high atomic number ions over the hydrocarbon matrix indicates ionic domains should exhibit strong amplitude contrast. Imaging of ionic domains should therefore employ zero defocus and small objective aperture conditions.

Two other important factors should be considered in interpreting images.

1. Geometry. The image is a two-dimensional projection of the three-dimensional specimen. Figure 4 shows two possible geometries of domains in a matrix. If, as in Figure 4A, the domain thickness and film thickness are similar, the projected image is uncomplicated, and correct interpretation of the domain image is possible. In Figure 4B, however, the domains are randomly distributed and are much smaller than the film thickness so that the resulting projection will be nearly indistinguishable from random noise. For this reason very thin specimens must be prepared to study ionomers.

2. Radiation Damage. Molecules containing low atomic number atoms such as polymers may change their chemical structure rapidly in the electron beam under high-resolution conditions, making interpretation of these images questionable.[31] Clusters of heavy atoms, however, have been shown to remain approximately fixed during irradiation and, hence, are subject to more reliable interpretation.[32-34] Therefore, even though the polymer may be partially destroyed, the ionic clusters might be expected to remain.

## Experimental Section

**Instrumentation.** A JEOL 100CX transmission electron microscope with a scanning attachment (STEM) was operated at 40 kV for secondary electron imaging (SEI) and at 100 kV for transmission electron microscopy (TEM) experiments. Optical transforms were obtained on a Polaron optical bench.

A Porter Blum MT-2B ultramicrotome with a Cryokit attachment was used to obtain thin sections. At room temperature, sections were floated off on distilled water, and at low temperature, sections were removed from the diamond knife edge with a hair which was wetted with isopropyl alcohol.

A Rigaku-Denki small-angle X-ray camera was used to collect small-angle scattering data. Nickel-filtered Cu K$\alpha$ radiation was used with slit collimation. X-rays were detected by a scintillation counter equipped with a pulse height analyzer set according to the procedure of Taggart.[35] Samples were run in a nickel-foil cell filled with helium.

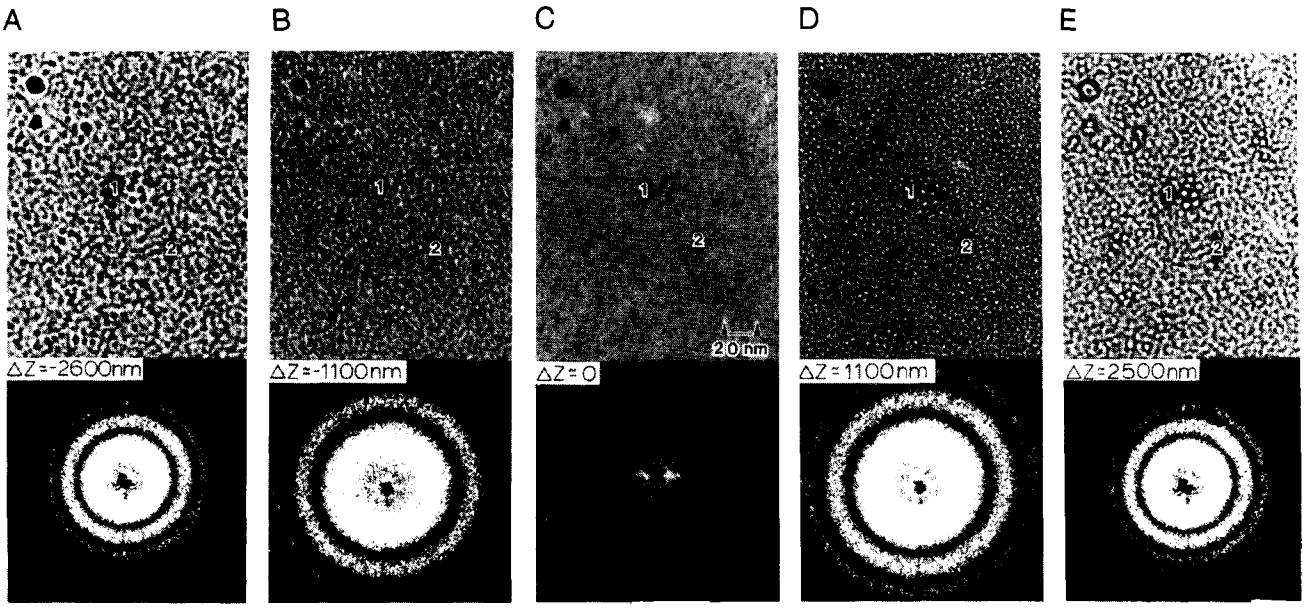


**Figure 3.** Bright field through-focus series of a carbon film. Defocus was measured from the optical transforms. Arrow 1 shows small particles changing size and contrast with defocus and arrow 2 points to featureless regions of the carbon film which develop structure under defocus conditions.

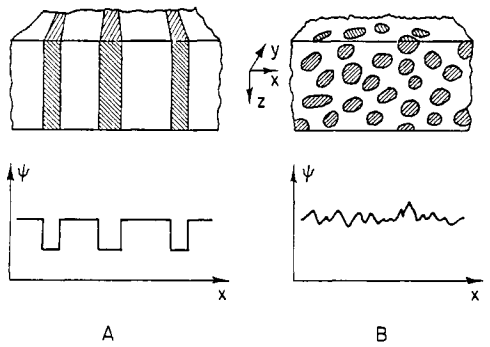


**Figure 4.** Two possible geometries of domains in a matrix. The projected potential of configuration A is interpretable while that of B is identical with random noise.

**Polymers.** A copolymer of 6.1 mol % methacrylic acid and ethylene was supplied by du Pont. Its neutralization has been previously described.[38]

Polypentenamer (supplied by Goodyear) was treated by Rahrig's sulfonation method to sulfonate 15 mol % of the double bonds.[37] The sulfonated polypentenamer was converted to the sodium or cesium salt before precipitation from solution since the acid form is unstable.

Sulfonated polystyrene (23 mol %) (supplied by Exxon) was dissolved in tetrahydrofuran and neutralized with cesium hydroxide.

The cesium salt of a 1 mol % sulfonated EPDM composed of approximately 54% ethylene, 43% propylene, and 3% diene was also supplied by Exxon.

**Sample Preparation.** Films of the E–MAA copolymer were prepared by placing a few drops of a 0.1% solution in xylene onto water or 2% MOH in water (M = Na, K, Cs) at 70 °C following the technique of Davis.[10]

Thin sections of the E–MAA copolymer, EDPM, and polypentenamer were microtomed at −75 °C. The more rigid sulfonated polystyrene could be microtomed at room temperature. All samples were desiccated until observation.

Film thicknesses were estimated by producing contamination marks on the entrance and exit surfaces of the film with a 3-nm probe of electrons in the STEM mode. The sample was then tilted 40° from the optic axis and the distance between the contamination marks measured in TEM.

Some samples were treated by immersing in a solution of 2 M CsOH in methanol and washing in methanol five times. Vapor phase staining with chloroform was done by placing grids containing sections on a screen 1 cm above chloroform, which had been carefully distilled over phosphorus pentoxide to remove stabilizers, for 1 h.

Sulfonated EPDM was stained for 2 h with osmium tetraoxide by placing the sections 3 cm above a 2% solution of $OsO_4$ in water.

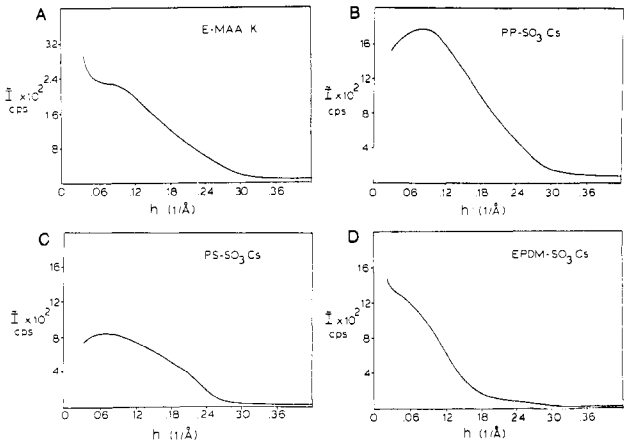


**Figure 5.** Smeared SAXS of (A) potassium salt of E–MAA copolymer, (B) cesium salt of sulfonated polypentenamer, (C) cesium salt of sulfonated polystyrene, and (D) cesium salt of sulfonated EPDM.

## Results and Discussion

**SAXS.** Figure 5 shows the smeared SAXS curves of the four ionomers. Since a 200-$\mu$m slit was used to define the beam, these curves do not represent the true intensity profiles but are useful for comparison. The sulfonated polypentenamer, sulfonated polystyrene, and E–MAA copolymer contain approximately the same number of ions per volume and show a rather broad scattering peak corresponding to a Bragg spacing of approximately 7 nm. The sulfonated EPDM contains fewer ionic groups and shows a broad peak centered at a slightly higher spacing of approximately 10 nm. The cesium salts have much higher scattering intensities than the potassium salt of E–MAA since there is a larger electron density fluctuation associated with the domains. As mentioned above, several cluster models may be applied to fit these data but un-

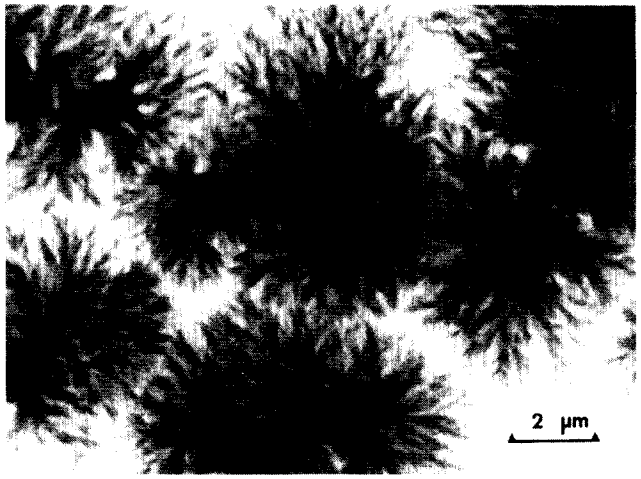


**Figure 6.** E–MAA copolymer cast from xylene onto water at 70 °C. The sample shows a spherulitic morphology similar to that of low-density polyethylene.

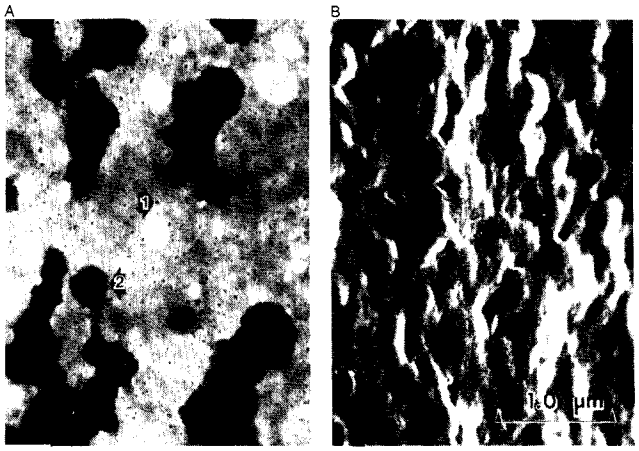


**Figure 7.** E–MAA copolymer cast from xylene onto 2% KOH solution. (A) TEM shows small crystals (arrow 1) and larger spheres (arrow 2) which SEI of a gold decorated film (B) shows are surface features.

ambiguous discrimination among the models is not possible by X-ray scattering.

**Electron Microscopy.** Results from the unstained cast or microtomed films will be given first, followed by three techniques used to attempt to increase amplitude contrast.

**Solvent-Cast Films.** As Davis et al. reported, a spherulitic film was formed by placing drops of the acid or salt form of E–MAA onto water (Figure 6). This morphology is similar to that of low-density polyethylene, suggesting that no ionic clustering occurs in this case.[10] When the ionomer is cast onto dilute solution of base (Figure 7A), however, a nonspherulitic film is formed with two major features.

1. Spherical regions approximately 1 μm in diameter are produced, probably by the ionomer acting as a surfactant encompassing droplets of polar solvent. SEI of a gold-coated film (Figure 7B) shows that these are surface features which are not present in the highly transparent bulk polymer since they would scatter light strongly.

2. Irregular electron dense features of about 2–20 nm, which were supposed by Davis to be ionic domains, are found throughout the films (Figure 8).

Figure 8A,B is a bright field–dark field pair showing that the 2–20-nm irregular features are actually crystals of the base solution on which the film was cast. The crystals lose mass rapidly upon irradiation, leaving voids (Figure 8C,D).

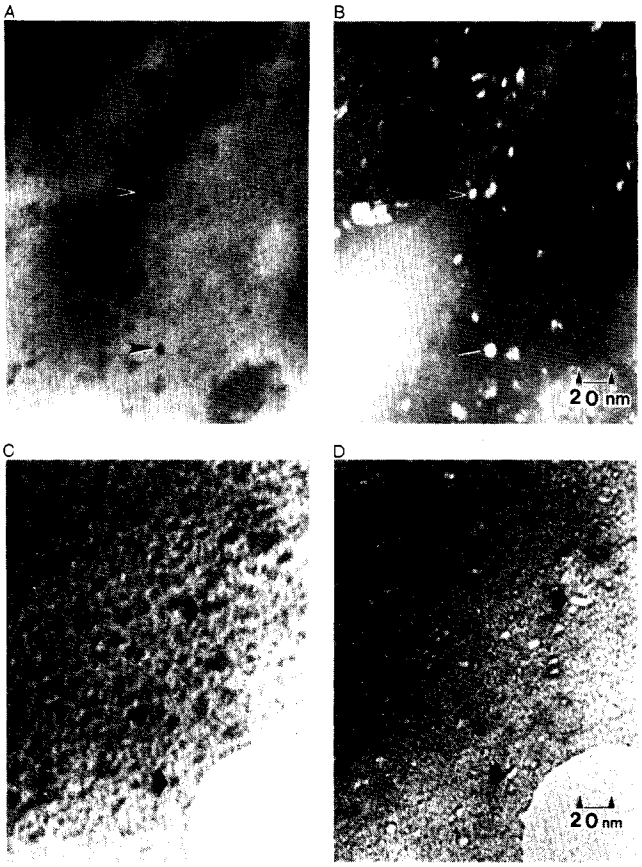


**Figure 8.** Higher magnification of the crystals shown in Figure 7 in bright field (A), in dark field (B) using the $k = 3.4$ nm$^{-1}$ ring of the crystalline diffraction pattern, in bright field before mass loss (C), and in bright field after radiation damage (D). Parts C and D are taken with slight underfocus to enhance contrast.

These features are obviously not representative of the bulk morphology of the sample and obscure any possible observations of ionic domains.

Ionomers are generally difficult to solvent cast because they usually require a polar and a nonpolar solvent to dissolve. The two or more solvents have different evaporation rates and surface tensions, resulting in large-scale phase separation during film casting which does not reflect the true bulk ionomer morphology. Finding the correct solvent pair and a casting surface which will not leave 1–5-nm inhomogeneities in the film may not be possible for these polymers.

**Microtomed Sections.** Due to thermal instabilities in the microtome at low temperatures, sections of the flexible ionomers range in thickness from 100 to 500 nm. This results in the situation shown in Figure 4B since ionic domains are expected to be 1–5 nm in diameter. Sections cut at room temperature are thinner (30 nm or greater) but still an order of magnitude thicker than the expected domain size, and the effect of polar solvents used in removing the sections from the knife on the domain structure is not well understood. Therefore, one is still faced with trying to observe small domains in a relatively thick film by searching for isolated thin areas. As Figure 9 shows, microtomed sections of three of the polymer salts (E–MAA, sulfonated polypentenamer, and sulfonated polystyrene) at approximately zero defocus show no contrast other than the intrinsic small-scale (<1 nm) phase contrast expected from an otherwise featureless film. The sulfonated EPDM shows approximately 300-nm electron dense regions which comprise about 6 vol % of the sample and are apparently not present in the absence of ionic groups.

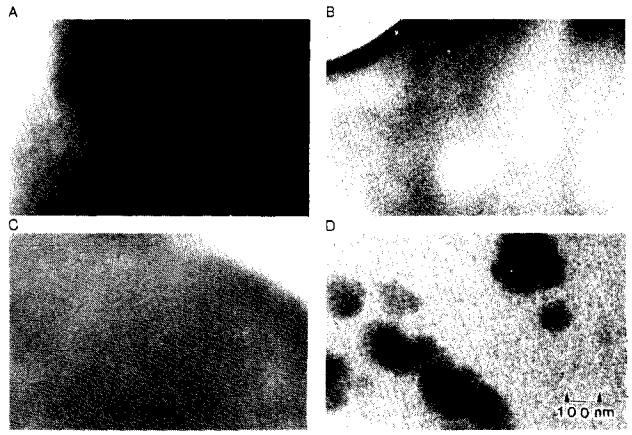


**Figure 9.** Microtomed sections of the ionomers: (A) potassium salt of E–MAA copolymer; (B) cesium salt of sulfonated polypentenamer; (C) cesium salt of sulfonated polystyrene; (D) cesium salt of sulfonated EPDM. All are at approximately zero defocus and show no amplitude contrast attributable to ionic domains of the size expected from SAXS.

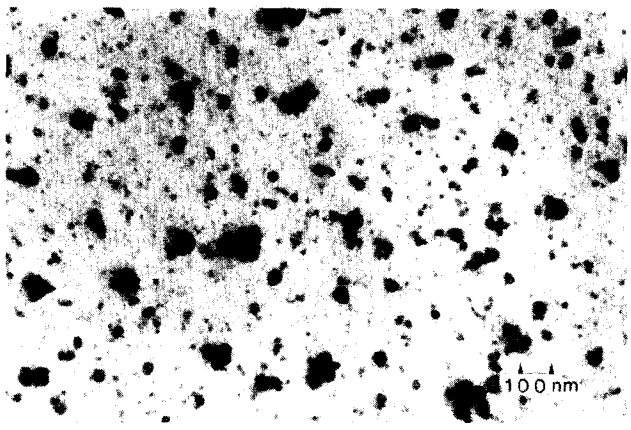


**Figure 10.** Crystals of CsOH and other surface artifacts produced by solution staining of a sulfonated polystyrene film in 2 M CsOH.

A possible explanation for this is an inhomogeneous distribution of the diene monomer, leading to large regions which are relatively highly sulfonated.

Since insufficient amplitude contrast was found in the unstained films, several techniques were used to try to increase the electron density in the ionic regions.

1. Immersing sulfonated PS in 2 M CsOH resulted in features shown in Figure 10. This micrograph shows crystals of CsOH deposited on the surface and other large surface features probably due to swelling of the polymer by the solvent followed by evaporation of the solvent. A similarly treated section of polystyrene did not show these features. Since ionic domains are expected to be extremely small and randomly spaced, it is doubtful that such solvent staining techniques can yield unambiguous results.

2. Figure 11 shows that sections exposed to carefully distilled chloroform vapor contained MCl microcrystals (M = Na, K, or Cs, depending on which cation was present in the ionomer). The 6–10-nm cubic crystals were nucleated randomly throughout the polymer and may indicate the presence of numerous small ionic domains which could serve as nucleation sites. From stoichiometric calculations on the E–MAA copolymer Na salt, a NaCl crystal 6 nm on a side would require only the Na atoms in a 16-nm cube of polymer and would occupy approximately 5 vol % of the polymer film. The crystals observed in this copolymer satisfy these criteria and so could be formed from the ions present in the 100% neutralized ionomer containing no excess ions. The acid form of E–MAA was not affected by exposure to chloroform. Sulfonated polypentenamer and EPDM also showed similar crystals when exposed to chloroform. Sulfonated polystyrene did not, probably because of low ion mobility in the glassy polymer.

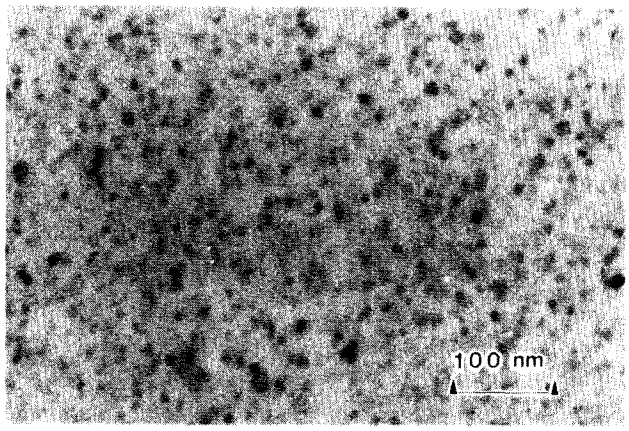


**Figure 11.** E–MAA ionomer microtomed section showing 6–10-nm cubic KCl crystals after treating with chloroform vapor.

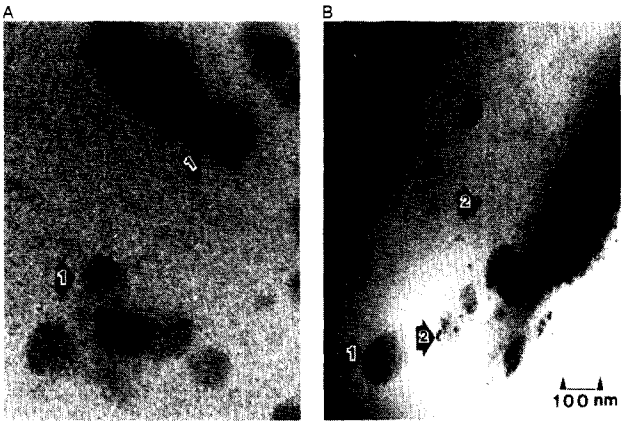


**Figure 12.** EPDM microtomed sections: (A) unstained, showing 300-nm phase separation (arrows 1); (b) stained with $OsO_4$, showing approximately 3-nm electron dense regions (arrows 2) primarily in the more electron dense phase.

3. Since sulfonated EPDM contains double bonds only at the ionic groups, staining these bonds with osmium tetraoxide should increase both the apparent size and electron density of any ionic domains. Figure 12 shows an unstained and a stained section. In the stained section electron-dense and a of 6 nm or less appear within the larger 300-nm phase-separated regions of the polymer. These small clusters probably correspond to the ionic domains in this polymer, but due to the 300-nm-scale phase separation, the domains may be different from those in other ionomers. Unfortunately, the section thickness prohibits an accurate determination of the size distribution or the detailed shape of these domains and hence the selection of the most appropriate model of domain structure. Most of the domains, however, appear to be spherical and smaller than 3 nm in diameter.

## Conclusions

Solvent-cast ionomer films have produced several interesting artifacts but no reliable information about the size or shape of ionic domains in the bulk. Microtomed sections of four ionomers do not suffer from these preparative artifacts but show no definitive features which can

be interpreted as ionic domains for unstained films, although SAXS indicates the presence of clusters. This leads to several possibilities.

1. Most ionic domains are less than 2 or 3 nm in diameter and, therefore, might not be detectable in relatively thick sections. This would apparently rule out the presence of lamellae of ions with lateral dimensions or thickness of 3.5 nm, as proposed by Roche.[6]

2. The ion clusters are diffuse, resulting in very low amplitude contrast. This possibility does not limit the size or shape of the cluster.

The results of the amplitude contrast imaging with osmium tetraoxide stained sulfonated EPDM indicate that ionic domains probably do exist but average less than 2 or 3 nm in diameter. Hence, ultrathin specimens may make direct observation possible. We are preparing an ionomer based on styrene which will have a stainable double bond at each ionic group, will not have any phase separation other than ionic clusters, and can be microtomed at room temperature. We hope this polymer can be prepared in suitably thin films to allow determination of the structure of the domains.

**Acknowledgment.** We thank Dr. H. Nakamura for help in neutralizing several of the ionomers. Acknowledgment is made to the National Science Foundation for financial support (Grants DMR80-12724 (E.L.T.) and DMR78-09761 (W.J.M.), Polymers Program) and to the donors of the Petroleum Research Fund, administered by the American Chemical Society, for partial support of this research. The use of the facilities of the Materials Research Laboratory at the University of Massachusetts is also gratefully acknowledged.

## References and Notes

(1) Holliday, L. "Ionic Polymers"; Applied Science Publishers: London, 1975; Chapter 2.
(2) Wilson, F. C.; Longworth, R.; Vaughn, D. J. *Polym. Prepr., Am. Chem. Soc., Div. Polym. Chem.* **1968**, *9*, 505.
(3) Delf, B. W.; MacKnight, W. J. *Macromolecules* **1969**, *2*, 309.
(4) Marx, C. L.; Caulfield, D. F.; Cooper, S. L. *Macromolecules* **1973**, *6*, 344.
(5) Kao, J.; Stein, R.; MacKnight, W. J.; Taggart, W. P.; Cargill, C. S., III *Macromolecules* **1974**, *7*, 95.
(6) Earnest, T.; Handlin, D.; Higgins, J.; MacKnight, W. J. *Macromolecules* **1981**, *14*, 192.
(7) Roche, E. J.; Stein, R. S.; MacKnight, W. J. *J. Polym. Sci., Polym. Phys. Ed.* **1980**, *18*, 1035.
(8) Roche, E. J. Ph.D. Thesis, University of Massachusetts, 1978.
(9) MacKnight, W. J.; Taggart, W. P.; Stein, R. S. *J. Polym. Sci., Polym. Symp.* **1974**, *45*, 113.
(10) Davis, H. A.; Longworth, R.; Vaughn, D. J. *Polym. Prepr., Am. Chem. Soc., Div. Polym. Chem.* **1968**, *9*, 534.
(11) Marx, C. L.; Koutsky, J. A.; Cooper, S. L. *J. Polym. Sci., Polym. Lett. Ed.* **1971**, *9*, 167.
(12) Phillips, P. J. *J. Polym. Sci., Polym. Lett. Ed.* **1972**, *10*, 443.
(13) Pineri, M.; Meter, C.; Bourret, A. *J. Polym. Sci., Polym. Phys. Ed.* **1975**, *13*, 1881.
(14) Jouffrey, B.; Dorignac, D.; Tanaka, M. *Chem. Scr.* **1978–1979**, *14*, 63.
(15) Hansen, K. *Adv. Opt. Electron Microsc.* **1971**, *4*.
(16) Erickson, H. P. *Adv. Opt. Electron Microsc.* **1973**, *5*.
(17) Cowley, J. M. "Diffraction Physics"; North-Holland Publishing Co.: Amsterdam, 1975.
(18) Thomas, E. L.; Roche, E. J. *Polymer* **1979**, *20*, 1413.
(19) Roche, E. J.; Thomas, E. L. *Polymer* **1981**, *22*, 333.
(20) Glauber, R. *Lect. Theor. Phys.* **1958**, *1*, 315.
(21) Wilkes, G. L.; Samuels, S. L.; Crystal, R. *J. Macromol. Sci., Phys.* **1974**, *B10*, 203.
(22) Koutsky, J. A.; Hun, N. V.; Cooper, S. L. *J. Polym. Sci., Polym. Lett. Ed.* **1970**, *8*, 353.
(23) Chang, A. L.; Thomas, E. L. *Adv. Chem. Ser.* **1979**, *No. 176*, 31.
(24) Yeh, G. S. Y.; Geil, P. H. *J. Macromol. Sci., Phys.* **1967**, *B1*, 235.
(25) Yeh, G. S. Y. *Crit. Rev., Macromol. Chem.* **1972**, *1*, 173.
(26) Klement, J. J.; Geil, P. H. *J. Macromol. Sci., Phys.* **1972**, *B6*, 31.
(27) Carr, S. H.; Geil, P. H.; Baer, E. *J. Macromol. Sci., Phys.* **1968**, *B7*, 13.
(28) Frank, W.; Goddar, H.; Stuart, H. A. *J. Polym. Sci., Part C* **1967**, *5*, 711.
(29) Siegman, A; Geil, P. H. *J. Macromol. Sci., Phys.* **1970**, *B9*, 239.
(30) Luch, P.; Yeh, G. S. Y. *J. Appl. Phys.* **1972**, *43*, 4326.
(31) Klug, A. *Chem. Scr.* **1978–1979**, *14*, 291.
(32) Klug, A. *Chem. Scr.* **1978–1979**, *14*, 245.
(33) Wall, J. S. *Chem. Scr.* **1978–1979**, *14*, 271.
(34) Hashimoto, H.; Kumao, A.; Endoh, H. *Symp. Int. Cong. Electron Microsc., 9th* **1978**, *3*, 244.
(35) Taggart, W. P. Ph.D. Thesis, University of Massachusetts, 1973.
(36) Schmidt, P. W. *Acta Crystallogr.* **1965**, *19*, 938.
(37) Rahrig, D. B. Ph.D. Thesis, University of Massachusetts, 1978.
(38) MacKnight, W. J.; McKenna, L. W.; Read, B. E. *J. Appl. Phys.*, **1967**, *38*, 4208.

# Nitroxide Spin Probe Studies in a Block Copolymer

**I. M. Brown**

*McDonnell Douglas Research Laboratories, St. Louis, Missouri 63166.*
*Received October 29, 1980*

ABSTRACT: Pulsed and CW EPR studies of a block copolymer of bisphenol A carbonate (BPAC) and dimethylsiloxane (DMS) containing a nitroxide spin probe are described. Below 220 K the line shapes consist of a single broad-line nitroxide spectrum which can be characterized by a motional correlation time $\tau_c > 10^{-7}$ s, whereas above 380 K the line shapes have the form of a typical three-line motionally narrowed nitroxide spectrum with the values $\tau_c < 10^{-9}$ s. At intermediate temperatures (220–380 K), the results of pulsed EPR experiments verify that the observed spectra are a superposition of a fast-phase spectrum ($\tau_c < 10^{-9}$ s) and a slow-phase spectrum ($\tau_c > 10^{-7}$ s). The fast phase is identified with the spin probes located in rubbery DMS block environments, and the slow phase corresponds to spin probes located in domains of associated BPAC blocks and/or in regions of DMS blocks whose segmental motions are restricted by the constraints imposed by the domains. The temperature dependence of the fast-phase fraction shows a good fit to a Gaussian distribution of the transition temperatures which describe the sudden onset of the motional narrowing. This distribution, which has a center at 374 K and a half-width of 88 K, is considered to be a measure of the distribution of polymeric main-chain segmental motional activity.

In this paper we describe the results of a study of the main-chain segmental motions associated with the glass transitions in the random alternating block copolymers of bisphenol A carbonate (BPAC) and dimethylsiloxane

0024-9297/81/2214-0801$01.25/0 